The Astrophysical Journal, 859:9 (11pp), 2018 May 20 https://doi.org/10.3847/1538-4357/aab3e2

Recovering the Physical Properties of Molecular Gas in Galaxies from CO SLED Modeling

J. Kamenetzky[1], G. C. Privon[2,3,4], and D. Narayanan[4,5]
[1] Westminster College, 1840 S 1300 E. Salt Lake City, UT 84105 USA; jkamenetzky@westminstercollege.edu
[2] Instituto de Astrofísica, Facultad de Física, Pontificia Universidad Católica de Chile, Casilla 306, Santiago 22, Chile
[3] Departamento de Astronomía, Universidad de Concepción, Casilla 160-C, Concepción, Chile
[4] Department of Astronomy, University of Florida, 211 Bryant Space Sciences Center, Gainesville, FL 32611, USA
[5] Cosmic Dawn Center (DAWN), Niels Bohr Institute, University of Copenhagen, Juliane Maries vej 30, DK-2100 Copenhagen, Denmark
Received 2017 October 26; revised 2018 February 3; accepted 2018 March 2; published 2018 May 16

Abstract

Modeling of the spectral line energy distribution (SLED) of the CO molecule can reveal the physical conditions (temperature and density) of molecular gas in Galactic clouds and other galaxies. Recently, the *Herschel Space Observatory* and ALMA have offered, for the first time, a comprehensive view of the rotational $J = 4-3$ through $J = 13-12$ lines, which arise from a complex, diverse range of physical conditions that must be simplified to one, two, or three components when modeled. Here we investigate the recoverability of physical conditions from SLEDs produced by galaxy evolution simulations containing a large dynamical range in physical properties. These simulated SLEDs were generally fit well by one component of gas whose properties largely resemble or slightly underestimate the luminosity-weighted properties of the simulations when clumping due to nonthermal velocity dispersion is taken into account. If only modeling the first three rotational lines, the median values of the marginalized parameter distributions better represent the luminosity-weighted properties of the simulations, but the uncertainties in the fitted parameters are nearly an order of magnitude, compared to approximately 0.2 dex in the "best-case" scenario of a fully sampled SLED through $J = 10-9$. This study demonstrates that while common CO SLED modeling techniques cannot reveal the underlying complexities of the molecular gas, they can distinguish bulk luminosity-weighted properties that vary with star formation surface densities and galaxy evolution, if a sufficient number of lines are detected and modeled.

Key words: galaxies: ISM – ISM: molecules – submillimeter: ISM

1. Introduction

^{12}CO (hereafter, CO) serves as a tracer of cool molecular gas because of its high-dipole moment and low-lying rotational energy levels (e.g., Bolatto et al. 2013; Carilli & Walter 2013, and references therein). The ratios of its line emission allows us to determine the physical conditions (temperature and density) of the molecular gas (e.g., Weiß et al. 2007; Sliwa et al. 2012; Bayet et al. 2013; Meijerink et al. 2013; Greve et al. 2014; Papadopoulos et al. 2014; Schirm et al. 2014; Spilker et al. 2014; Daddi et al. 2015; Rosenberg et al. 2015; Xu et al. 2015; Kamenetzky et al. 2017; Strandet et al. 2017) and the absolute values of the emission (namely of $J = 1-0$) allows us to determine the total molecular gas mass (e.g., Bolatto et al. 2013, and references therein). Combined, this knowledge allows us to comment on the processes exciting the gas and therefore its relationship to star formation and galaxy evolution.

The *Herschel Space Observatory* opened a new observational window from 60 to 670 μm that allowed the study of spectral line energy distributions (SLEDs) through very high-J lines, thanks to the SPIRE Fourier Transform Spectrometer (FTS) and PACS. Prior to this, only the first few rotational transitions of CO were available to be studied through the atmosphere. Low-J CO, especially $J = 1-0$, is a well used tracer of total cold molecular gas, due to its low energy spacing (the $J_{\rm upper} = 1$ level is 5.53 K above ground) and strong dipole moment. The CO $J = 1-0$ line is generally optically thick and in local thermodynamic equilibrium (LTE). As one climbs up the CO ladder to measure emission from higher-J lines in a cloud or galaxy's SLED, the lines begin to fall from LTE (i.e., when $h\nu \gg kT$ as $E(J+1)$–$E(J)$ becomes larger with higher J), and non-LTE calculations of the level populations, optical depth, and resulting emission are required using a large velocity gradient (LVG) code like RADEX (van der Tak et al. 2007).

Because the temperature and density are degenerate parameters, a full examination of the parameter space using a grid method, Monte Carlo Markov Chain (MCMC), or nested sampling algorithm is important to characterize the shape of the parameter space and the uncertainty in any given parameter. The line luminosities of the $J = 4-3$ through $J = 13-12$ lines of CO, available for local galaxies with SPIRE, were discovered to be much more luminous than would be predicted by extrapolating the cold gas emission to higher-J lines, leading observers to often invoke a second, warmer component of gas to explain the luminous emission (see Kamenetzky et al. 2017 and references therein). The physical condition of the gas (as determined by the relative luminosities of the lines) is instructive to study as both the raw material for star formation and as indicating the effects of star formation via feedback such as radiative and turbulent excitation.

Tunnard & Greve (2016) studied the recoverability of physical conditions using the LVG code RADEX and two methods of χ^2 minimization: grid and MCMC. In essence, they asked, "If one produces a SLED in RADEX using a given set of physical conditions, can one fit the SLED and recover those original physical parameters?" They found that the parameters (temperature and density of the colliding partner, H_2) are only recovered to within half a dex, given the degeneracy between the parameters and some uncertainty in the modeled SLED (as one would have observationally). Including isotopologue

lines with isotopologue abundance ratio as a free parameter improves the constraints. Leroy et al. (2017) studied the ability of dense gas tracers (HCN, HCO^+, HNC, CS) and the first few lines of CO to distinguish changes in the dense gas fraction and median volume density for modeled emission from an ensemble of gas clouds with log-normal and power-law density distributions.

Their ensembles were combined one-zone models of molecular emission, with a specified distribution of densities, but all gas was taken to be isothermal and with a fixed optical depth (and therefore escape probability). Analytical models, however, are often limited in their ability to approximate the diverse range of conditions in integrated extragalactic observations, typically assuming, e.g., isothermal or isobaric conditions.

Galaxies are complex, with a diverse range of physical conditions, and in principle the observed SLED is a superposition of the sum of individual SLEDs originating from all of the CO-emitting gas in a galaxy. What has been missing, therefore, is an investigation into the recoverability of physical conditions from SLEDs using bona fide galaxy evolution simulations that contain a large dynamic range in physical properties. Here, we seek to do just that. Narayanan & Krumholz (2014) used smoothed particle hydrodynamics to perform idealized simulations of isolated and interacting galaxies, and then produced galaxy-integrated CO SLEDs given the physical conditions of the simulated gas. In this paper, we investigate whether fitting these theoretical SLEDs in the same manner as is done for typical observations recovers the average physical conditions in the gas. In Section 2, we describe the methods used to the produce the simulated galaxies, the simulated SLEDs, and the fitting of those SLEDs. Our results and conclusions are described in Sections 3–5.

2. Methods

2.1. Galaxy Evolution Simulations

Our basic strategy is to fit model SLEDs from theoretical simulations and compare the derived physical properties from these SLEDs to the actual gas physical properties from the simulations. The model SLEDs were derived in Narayanan & Krumholz (2014), and we defer the reader to that paper alongside Narayanan & Krumholz (2017) for details regarding the hydrodynamic and radiative transfer simulations; though, we summarize the salient points here.

Following Narayanan et al. (2011, 2012), we employ GADGET-3 (Springel & Hernquist 2002, 2003; Springel et al. 2005) hydrodynamic simulations of idealized galaxies in evolution. The galaxies are initialized as exponential disks following the Mo et al. (1998) formalism, and reside in live Hernquist (1990) dark matter halos. The gas is initialized as primordial, and metals form as the simulations evolve. The interstellar medium is modeled as multiphase, with clouds pressure-confined by hot ISM (McKee & Ostriker 1977). Star formation proceeds in this cold gas following a volumetric Schmidt (1959) star formation relation with index $N = 1.5$ (Kennicutt 1998; Kennicutt & Evans 2012). The ISM is pressurized via supernovae via an effective equation of state; here, we assume a modest pressurization $q_{\rm EOS} = 0.25$ (Springel et al. 2005). This said, tests by Narayanan et al. (2011) show that the thermal properties of the ISM in the molecular phase are relatively insensitive to these choices.

In order to simulate a diverse range of physical conditions, we concentrate in this work on major binary galaxy mergers, with total baryonic mass $M_{\rm bar} = 3.1 \times 10^{11}$. The mergers are all identical on initialization, though they vary in their orbits. The physical properties of these galaxies are summarized in Table 1 of NK14, and in particular here we focus on models z0d4o, z0d4l, and z0d4e. The varying orbital angle impacts the strength of the nuclear starburst upon final coalescence, and therefore the physical properties of the molecular ISM during the most heavily star-forming phases.

The CO abundance depends on the carbon abundance, set to $X_C = 1.5 \times 10^{-4}\ Z/Z_\odot$ ($Z_\odot = 0.02$), and the semi-analytic model of Wolfire et al. (2010) to determine the fraction of carbon locked into CO. This fraction varies by cell and simulation. Luminosity-weighted averages for each snapshot vary from about 25% to 85%.

2.2. Determining Bulk Physical Conditions

For each snapshot from the simulations, the physical properties of the SPH particles were projected onto an adaptive mesh with an octree memory structure. The neutral gas is assumed to all reside in giant, spherical, isothermal clouds of constant density. The surface density is directly calculated from the mass within a given oct cell, though (following Narayanan et al. 2011) we consider a floor surface density of $\Sigma_{\rm cloud} = 85\ M_\odot\ {\rm pc}^{-2}$, comparable to observed values of local GMCs (Solomon et al. 1987; Bolatto et al. 2008). The H_2 gas mass within these clouds is determined from the Krumholz et al. (2008, 2009a, 2009b) formalism that balances the photodissociation rate of H_2 molecules by Lyman–Werner band photons against the growth rate of molecules on dust grains.

We model the subresolution turbulent compression (or "clumping") of gas by scaling the volumetric densities by a factor $e^{\sigma_p^2/2}$, where σ_p is a factor related to the 1D Mach number of the gas

$$\sigma_p^2 \approx \ln(1 + 3M_{\rm 1D}^2/4), \quad (1)$$

where this factor derives from turbulent box simulations (Ostriker et al. 2001; Padoan & Nordlund 2002; Lemaster & Stone 2008). It is these rescaled densities that are used in calculating the collision rates for excitation, and therefore these densities that we use for comparison between simulations and mock observations. The effects on the densities are shown in Figure 1. The total mass is conserved.

While the physical conditions are calculated for every cell, because, observationally, the bulk of SLED modeling is done for unresolved galaxies, we compare to weighted averages of the physical properties (e.g., gas temperature, dust temperature, $\rho_{\rm H2}$) in our models. We examine both the mass-weighted and CO-luminosity-weighted[6] physical properties, and show these in Figure 2.

In each of these and subsequent figures, the different simulations are indicated by different colors and marker shapes. Within a simulation, different snapshots at different points in time correspond to different star formation surface densities. This quantity, $\Sigma_{\rm SFR}$, is the x-axis in the figures, used to examine trends with star formation activity. By visual comparison of the filled (luminosity-weighted) and open

[6] Our CO-luminosity weighting is summed over the first 10 rotational transitions.

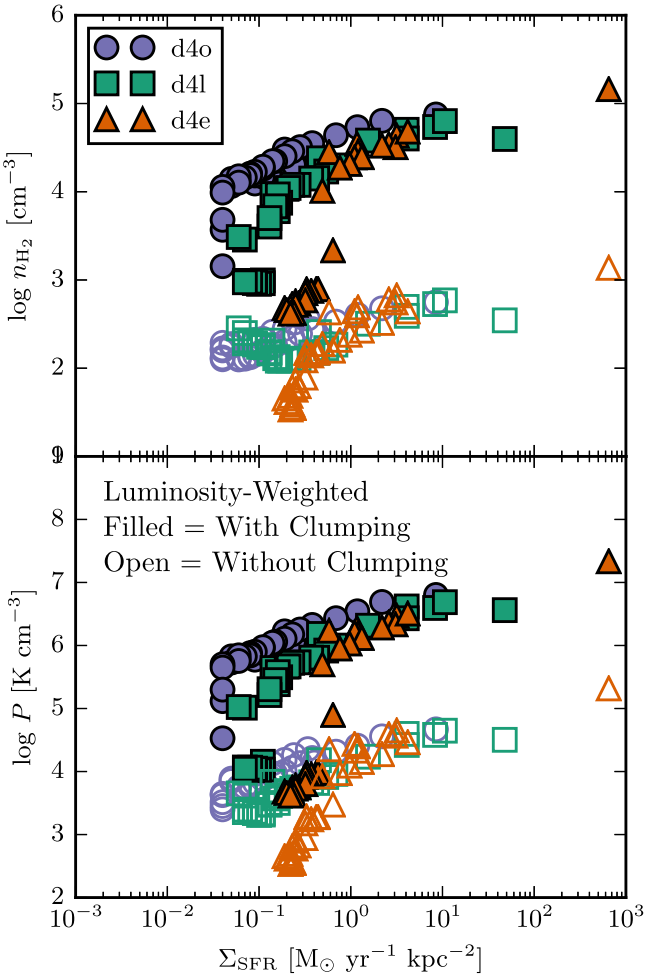

Figure 1. Effect of clumping on gas density (and subsequently, pressure). When producing the SLEDs with DESPOTIC, the collision rate coefficients were enhanced (Equation (1)) due to clumping associated with the nonthermal velocity dispersion. The filled markers are the associated (higher) mass-weighted densities and pressures due to this clumping. We note that Figure 4 of NK14, which is similar in form to our Figures 2 and 4, do not show the effect of clumping. The nonclumped parameters in open markers are not used for subsequent analysis.

(mass-weighted) markers, one can see that all of the parameters are generally higher when using the luminosity-weighted values. The difference is most pronounced for the low-Σ_{SFR} snapshots. The snapshots range from 5 to 10 Myr apart.

2.3. Galaxy-integrated SLEDs

"Observed" SLEDs were created for each simulation snapshot by taking the integrated flux measurements of each CO transition with $J_{upper} \leqslant 10$ from Narayanan & Krumholz (2014) and converting them into a line brightness. These calculations were done with DESPOTIC (Krumholz 2013), which operates under the escape probability formalism. Here, the thermal and radiative equilibrium are simultaneously solved for each model cloud. For all CO transitions, we assumed a total measurement error of 10%.

The galaxies were assumed to be unresolved and were placed at a fiducial redshift of $z = 0.05$ and are intended to emulate SLEDs measured with Herschel or ALMA observations (e.g., Kamenetzky et al. 2016; Lu et al. 2017). The SLED modeling requires an estimate of the size of the molecular gas; we used the area within a CO (1–0) contour of 1 K km s^{-1}. We also performed comparison fits using a luminosity-weighted area (which is typically much smaller than the "contour" area), but the choice of area did not significantly alter our results for the physical conditions of the molecular gas.

2.4. Line Fitting Procedure

The fitting of the "observed" SLEDs follows the procedure in Kamenetzky et al. (2014). We use the nested sampling algorithm MULTINEST (Feroz et al. 2009) and its python wrapper, PYMULTINEST (Buchner et al. 2014), to compare the "observed" SLEDs to those produced by the non-LTE code RADEX (van der Tak et al. 2007). As mentioned, the SLEDs themselves were produced using DESPOTIC, which introduces a minor inconsistency in our modeling. We address this further in Section 3. We use the same code as that used to fit actual extragalactic SLEDs observed by the *Herschel*-SPIRE FTS reported in Kamenetzky et al. (2017) and PYRADEXNEST (Kamenetzky 2018), which is available online.[7] We also utilize the PYTHON wrapper to RADEX and PYRADEX.[8]

Each RADEX model depends on four free parameters: the kinetic temperature (T_{kin}), volume density of the collision partner with CO (molecular hydrogen, n_{H_2}), column density of CO (N_{CO}) per unit linewidth, and the angular area filling factor ($\Phi < 1$), which linearly scales the fluxes produced by RADEX. The rotational level populations and optical depths of each line are iteratively determined, and then the intensities (as background-subtracted Rayleigh–Jeans equivalent radiation temperatures) are calculated using an escape probability method. We assume a background temperature of 2.73 K for the cosmic microwave background at $z = 0$. In PYRADEXNEST, for a given set of parameters $\boldsymbol{p}$, we minimize the negative log likelihood of the predicted RADEX model $I(\boldsymbol{p})$ given the measurements $\boldsymbol{x}$ and errors $\boldsymbol{\sigma}$ as

$$-\ln(\mathscr{L}) = \sum_i 0.5\ln(2\pi) + \ln(\sigma_i) + 0.5(x_i - I_i(\boldsymbol{p}))^2\sigma_i^{-2}. \quad (2)$$

In the above equation, $\mathscr{L}$ is the likelihood, x_i is the "measured" line intensity of a single CO transition, σ_i is total uncertainty in a single transition measurement (10% of x_i), and $I_i(\boldsymbol{p})$ the RADEX-modeled line intensity for that transition given the parameters $\boldsymbol{p} = [T_{kin}, n_{H2}, N_{CO}, \Phi]$, described in the preceding paragraph.

In practice, a few other galaxy-specific parameters are set in the modeling. We assume a linewidth of 250 km s^{-1}; the total emission scales with this quantity, while the physical conditions (temperature and density) do not. The optical depth and escape probability in RADEX depend only on the column density per unit linewidth. Therefore, our total integrated line intensities must be divided by a linewidth for comparison to RADEX. A different choice of linewidth therefore scales the total integrated emission, which one must use to calculate the total column density and then total mass. As we are only interested in temperature and density, our results do not depend on the choice of assumed linewidth for the line fitting procedure.

We also place three binary priors on the likelihood calculation. The prior is one if the simulated parameters satisfy

[7] https://github.com/jrka/pyradexnest
[8] https://github.com/keflavich/pyradex

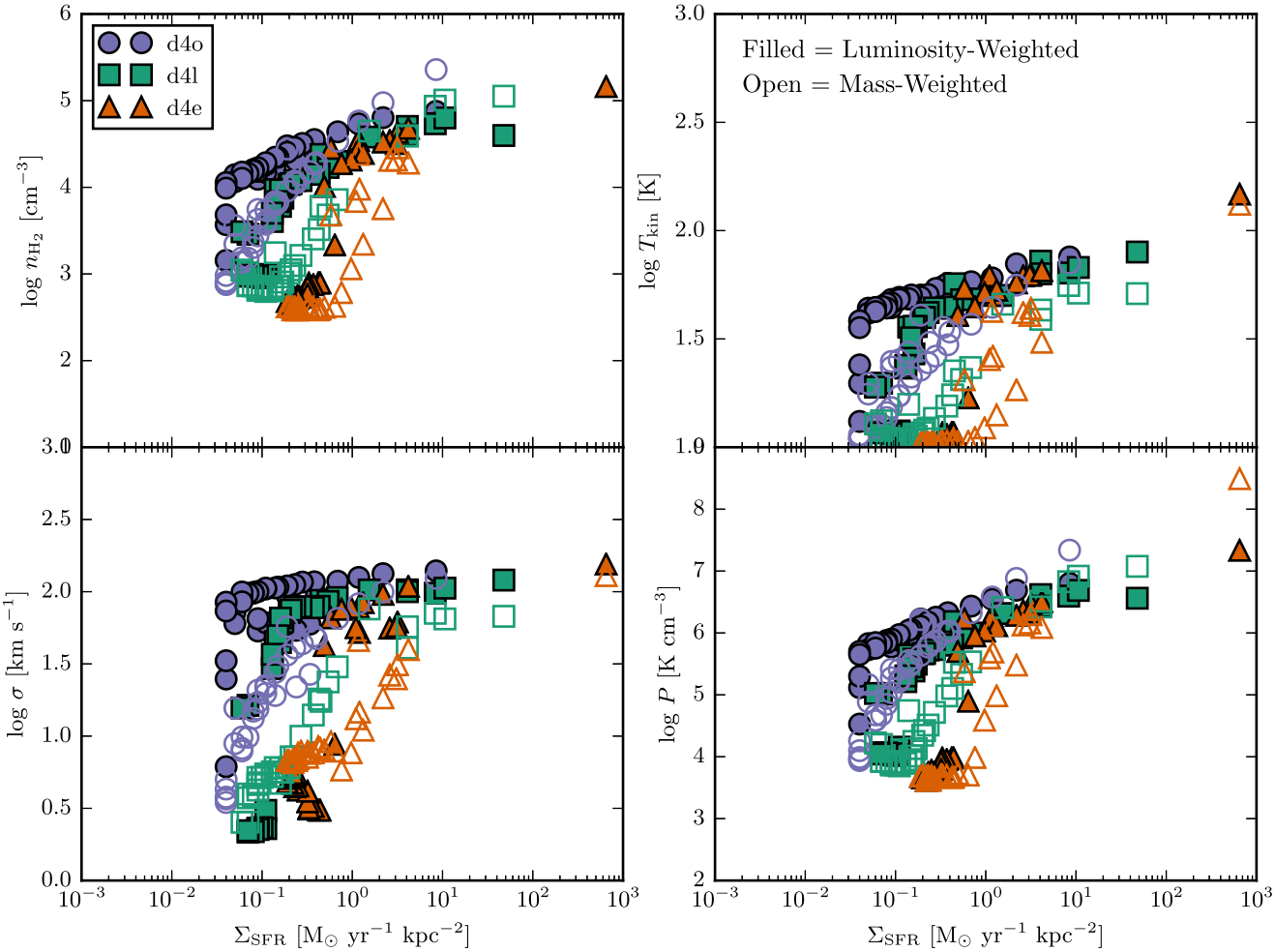

Figure 2. Summary of the luminosity-weighted (filled) and mass-weighted (open) parameters from the SPH grids. The values of all parameters are generally higher when considering the luminosity-weighted versions; the difference is most enhanced for the low-Σ_{SFR} snapshots. For both types of weighting, the density (and therefore also the pressure) are enhanced due to a clumping factor derived from the velocity dispersion (see Figure 1 and the associated explanation).

all three conditions, listed next to ensure physically plausible solutions, and zero if the simulated parameters violate any one condition. The first two conditions are an upper limit of 3×10^{12} $M_\odot$ on the total mass and a maximum length of 10 kpc. Finally, due to the limits of the escape probability formalism used by RADEX, we only include lines with optical depths between -0.9 and 100 in the likelihood calculation.

We focus primarily on what we will call the "physical conditions" of the gas, namely the kinetic temperature and the density. Because the temperature and density are degenerate, we also focus on the pressure $P/k = T_{kin} \times n_{H_2}$. For each of these three parameters, we marginalize over all other parameters to find a 1D probability distribution. From this distribution, we calculate a median value that represents our fitted estimate to compare to the grid value. We also calculate a 1σ width in the distribution to quantify the uncertainty in our fitted parameter.

3. Results

In Figure 3, we show a representative CO SLED, derived from the d4o simulation, along with the best-fit single-component model and uncertainties obtained following the procedure outlined above. The "observed" SLED is well-fit by the model, through the $J = 10-9$ line. Below we describe the differences between the simulated SLEDs and real galaxy SLEDs and how the best-fit model parameters correspond to the "true" values of the hydrodynamic simulations.

3.1. Differences between Simulated and Real SLEDs

Our model SLEDs exhibit a number of features that are unlike those observed in real galaxies. We find that our model SLEDs (through $J = 10-9$) are well-fit by one component of gas, whereas real galaxy-integrated SLEDs, such as those in Kamenetzky et al. (2017), require two components. In real galaxies, when combining ground-based data ($J = 1-0$ through usually $J = 3-2$) and SPIRE FTS line measurements ($J = 4-3$ through $J = 13-12$), the SLED is not well described by a single component of gas; the emission of the low-J lines is largely from cold gas, which falls off quickly by mid-J ($J = 4-3$ through $J = 6-5$) lines. A second, warmer component of gas is responsible for the emission of the mid-J lines and higher. When we tried to fit our model SLEDs with two components of gas, we found that the statistically best-fit SLED was one component anyway (with the second component being unconstrained, so long as it contributed negligibly to the fit).

Similarly, unlike real galaxy-integrated SLEDs, we find small uncertainties in the marginalized parameters (temperature, density, and pressure) when modeling as a single

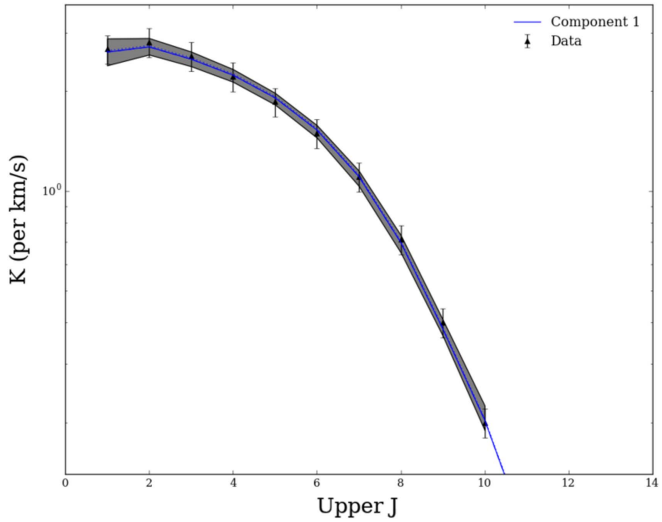

Figure 3. Sample CO SLED derived from the d4o simulation, showing the "observed" line fluxes and the best-fit model derived from the process described in Section 2.4. The straight blue line represents the best-fit SLED, and the shaded gray region represents the 1D marginalized parameter distribution uncertainties for each individual line intensity modeled from RADEX. CO SLEDs and best-fit models for the remainder of the simulations and snapshots are shown in Figures 9 and 10.

component. Although we include 10% error on the "observed" data points, the smooth behavior of the simulated SLED is often uniquely fit by a small set of parameter combinations. The median uncertainty for the density, temperature, and pressure was 0.2, 0.03, and 0.2 dex, respectively. For comparison, Tunnard & Greve (2016) found the recoverability of single component RADEX-created SLEDs to be about 0.5 dex without using isotopologues. In the two-component models of Kamenetzky et al. (2017), the warm component of gas is the best constrained and most comparable to this work; the uncertainty in the warm component pressure was about 0.3 dex (but 1.0 dex for the cold component; when modeled as two components, there is a larger degeneracy between parameters).

3.1.1. Comparison to Luminosity-weighted Parameters

Figure 4 compares the luminosity-weighted simulation parameters (filled symbols) to the PYRADEXNEST derived parameters from fitting the "observed" SLEDs (open symbols). As was shown in Figure 2, had we used the mass-weighted simulation parameters, the parameters (especially density) would be even lower and show a greater discrepancy between the "observed" parameters. Therefore, we focus on the luminosity-weighted parameters. However, there are still notable discrepancies, which we now investigate further.

Figure 5 shows the difference in fitted versus luminosity-weighted parameters for density, temperature, and pressure. The three simulations (shown in different colors), which have different merger properties, do not follow the same trends. Each one appears to have trends with $\Sigma_{\rm SFR}$ as the snapshots evolve over time. On this difference plot of PYRADEXNEST fitted value minus CO-luminosity-weighted simulation parameters, data points above the dashed zero line indicate snapshots for which our fitted values are higher than the grid values. For the most part, our fits underestimate the density, match or slightly overestimate the kinetic temperature, and underestimate the pressure. In some snapshots, however, we overestimate density and pressure instead.

In Figure 6, we show histograms of the differences between the luminosity-weighted and likelihood-fitted parameters. The fitted, statistical uncertainties themselves do not take into account the differences between using RADEX for fitting and DESPOTIC for the creation of the SLEDs.

The PYRADEXNEST best-fit models are highly weighted by and sensitive to the high-J line luminosity. We also examined the impact of comparing to simulation parameters weighted by each grid point's $J=8-7$ luminosity instead of total CO luminosity. Overall, the distributions are similar to those shown in Figures 4–7. However, for some of the lowest $\Sigma_{\rm SFR}$ snapshots ($<0.1\ M_{\odot}\ {\rm yr}^{-1}\ {\rm kpc}^{-2}$), the CO $J=8-7$ luminosity -weighted parameters are slightly higher than the total CO-luminosity-weighted parameters, and are better matched by our RADEX models.

3.1.2. Dependence on Number of Lines Modeled and Area

We also compared the values derived from modeling only up to $J=3-2$ instead of $J=10-9$. The result is much higher uncertainties in the parameters, but median values that align better with the luminosity-weighted parameters (see Figures 7 and 8). This is likely because most of the CO luminosity, even in simulation grid cells with extreme conditions, is in the low-J lines.

In our fitting algorithm, like in many others, the likelihood of a model RADEX SLED is weighted by the absolute value of the error bar of each data point. Assuming a constant relative error on each data point (e.g., 10% here) means that the relatively low-luminosity, high-J lines are significantly more heavily weighted in the fit. (Figures 9 and 10 demonstrate the large dynamic range of the SLEDs.) Fitting the whole SLED as one component seems to drive the fitted parameters to more diffuse, slightly hotter gas. Fitting only the low-J lines drives the fitted parameters to more dense, cooler gas that are more representative of the total luminosity-weighted parameters.

3.1.3. Dependence on Area

The mass depends on the product of the total column density and the assumed area of emission. If we change the area, the mass scales accordingly, but it does not significantly affect the physical conditions (temperature and density) because they are much more dependent on the shape of the SLED.

3.2. RADEX versus DESPOTIC

In Figures 9 and 10, we show the galaxy-integrated "observed SLEDs," the best-fit results from RADEX likelihood fitting, and the RADEX and DESPOTIC SLEDs that correspond to the temperature and density from the grid-weighted parameters.

For most of the lower $\Sigma_{\rm SFR}$ snapshots of d4e (Figure 9), the main differences in the grid and fit results seem to be the difference between RADEX and DESPOTIC (because the dashed DESPOTIC lines from the grids match the best fit from RADEX). For d4o (Figure 10), however, we find the galaxy-integrated SLEDs are not particularly consistent with either the RADEX or DESPOTIC SLED, corresponding to the luminosity-weighted parameters. Appendix D of Krumholz (2013) provides a detailed comparison to RADEX.

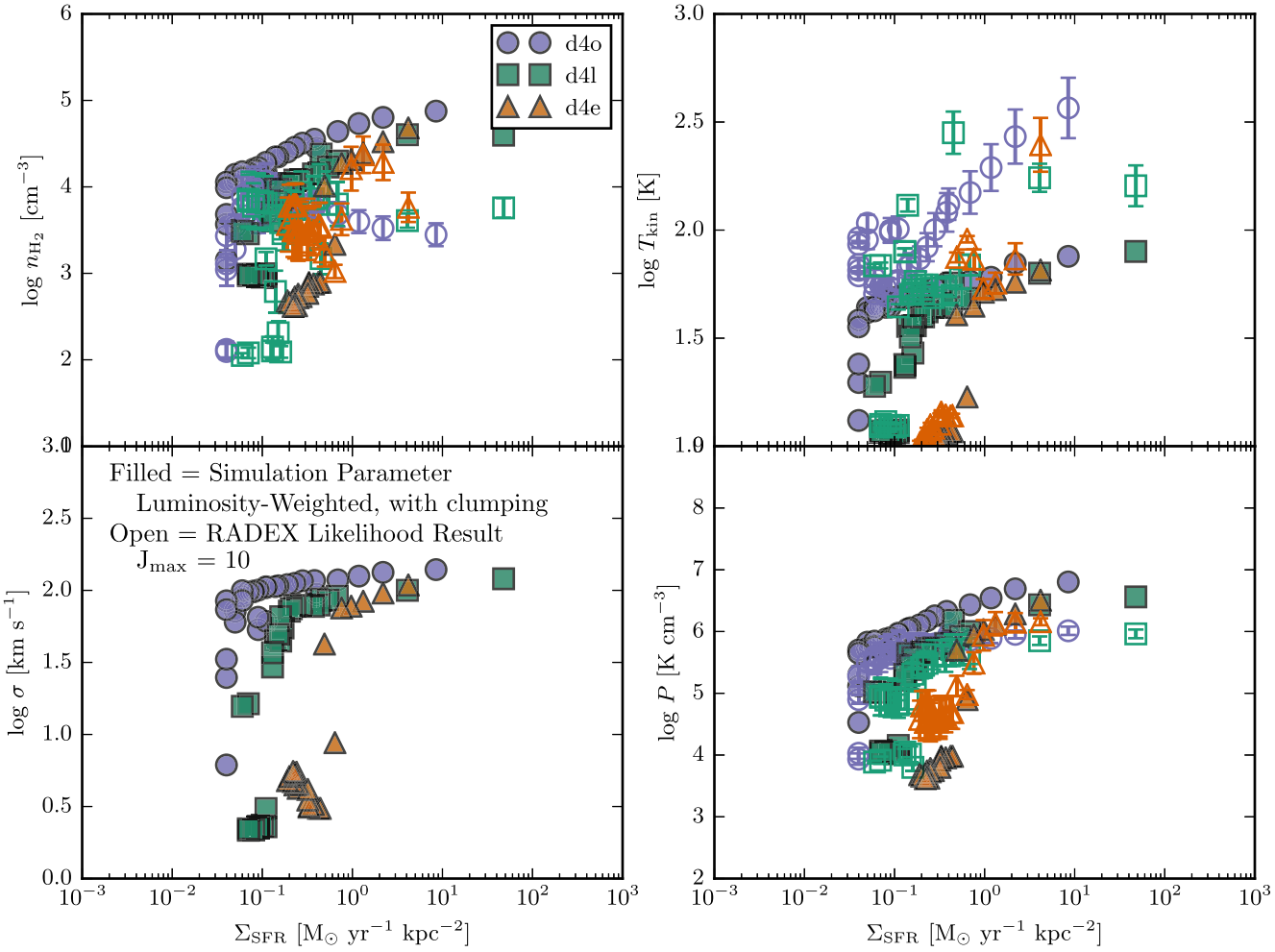

Figure 4. Comparison of the luminosity-weighted vs. likelihood-fitted parameters. Filled symbols are the simulation parameters; each simulation has a specific color and symbol. Open symbols of equivalent color/shape correspond to the PYRADEXNEST likelihood results.

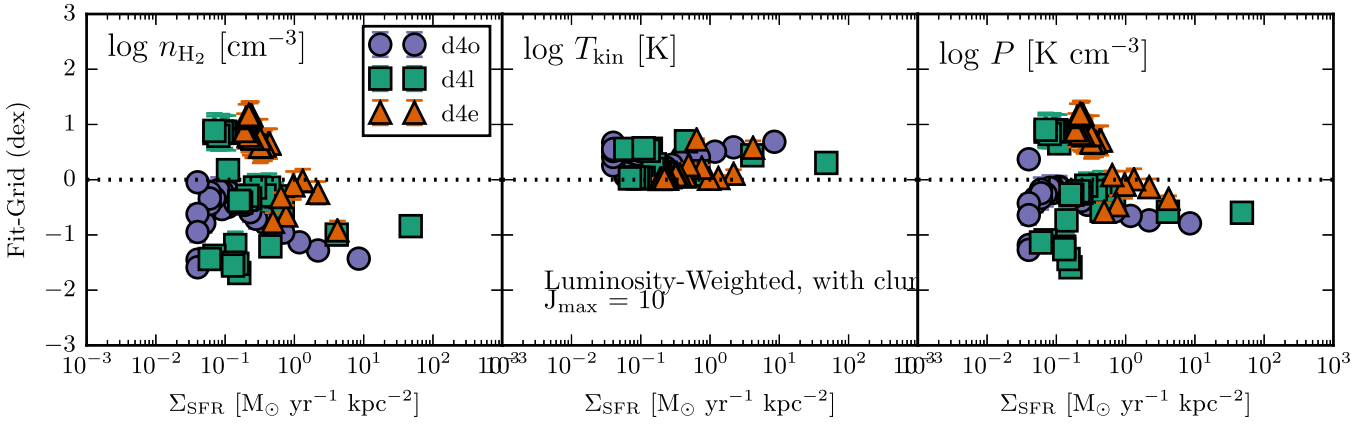

Figure 5. Differences between the luminosity-weighted vs. likelihood-fitted parameters.

4. Discussion

Fundamentally, we and others are attempting to answer the question: how good are our modeling techniques at determining the bulk physical properties of a complex ensemble of molecular gas? Even the highest resolution maps of nearby galaxies must convolve together a vast range of gas densities, temperatures, and dynamical properties. For all but the closest galaxies, line emission ratios must be constructed using a single integrated beam measurement or a map of only a handful of beams spanning the entire galaxy. We have chosen to model the lowest-resolution (one beam) scenario.

There are really two separate aspects (precision and accuracy) to the aforementioned question: (1) what are the inherent uncertainties in the modeling techniques, and (2) how accurately do the median quantities represent the actual quantities? To the first question, the work by Tunnard & Greve (2016) nicely showed that one should consider median

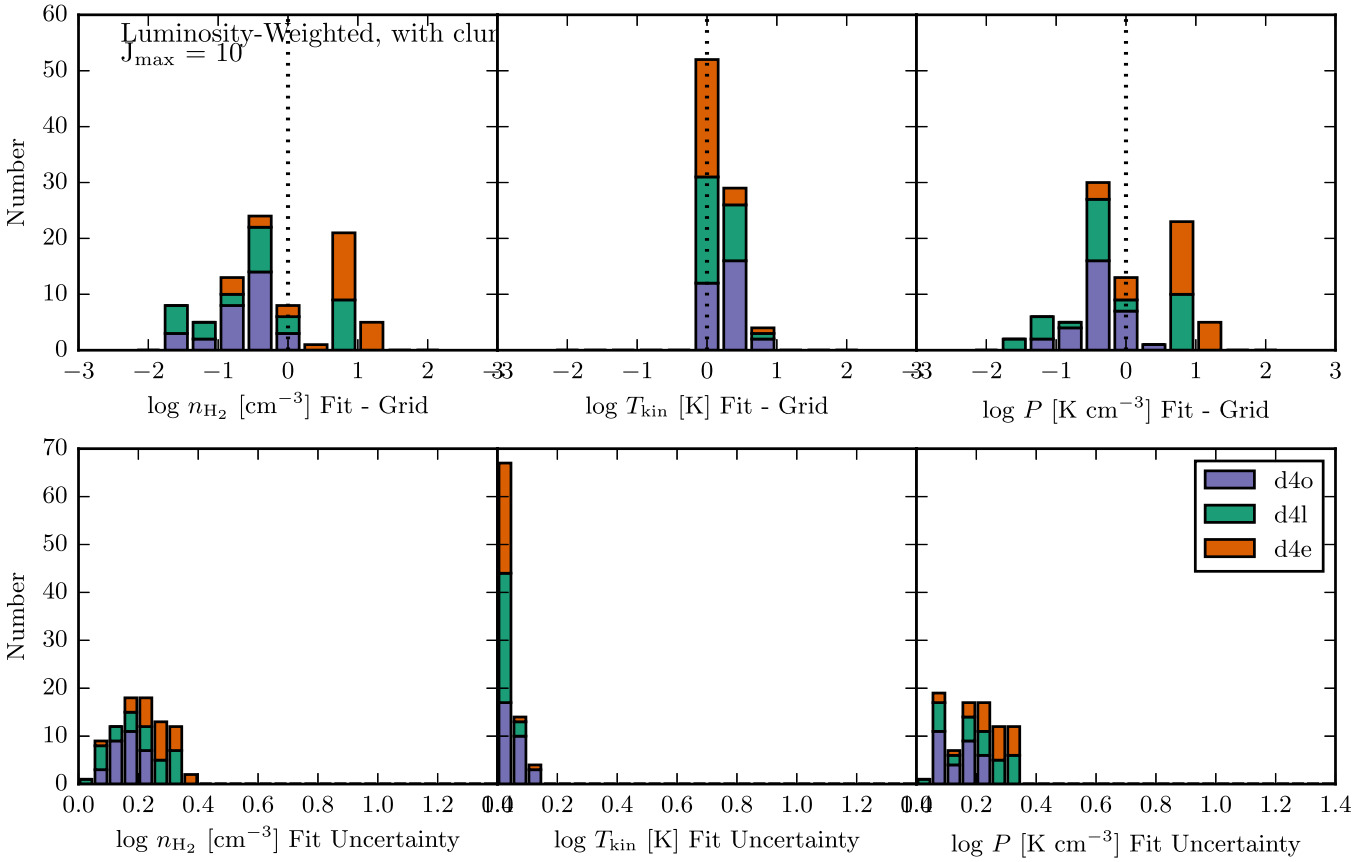

Figure 6. Top row: histogram of the difference between the luminosity-weighted and likelihood-fitted parameters. Bottom row: uncertainty (in dex) in the fitted parameters.

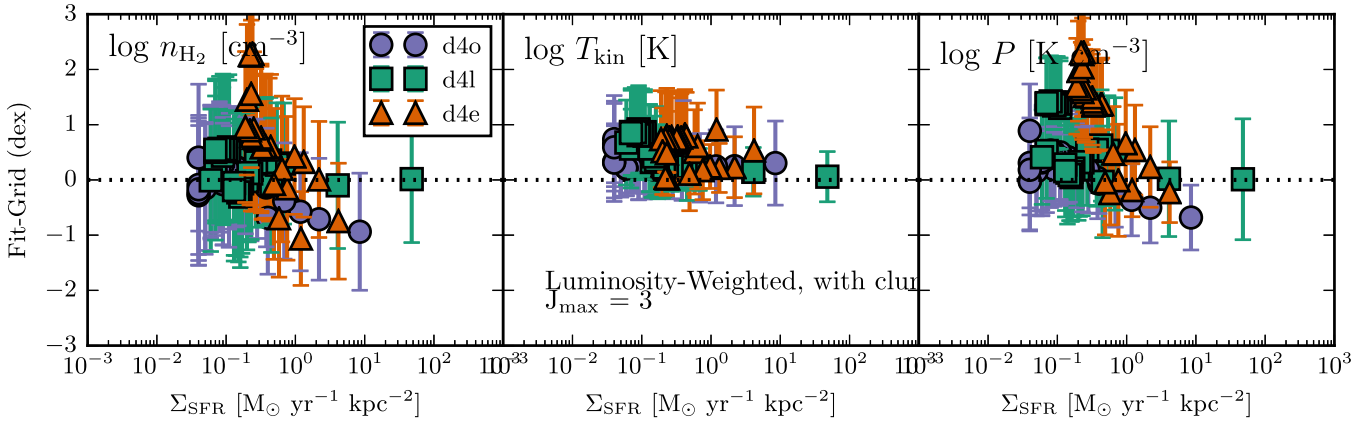

Figure 7. Differences between the luminosity-weighted vs. likelihood-fitted parameters, for only modeling up to $J = 3-2$.

quantities from LVG models (kinetic temperature, volume density, and velocity gradient) uncertain to at least 0.5 dex. Their simulated observational data included an optimistic uncertainty of 10%, the same as we do here, though they use three more lines than we do here (up to $J = 13-12$). Our approach differs from Tunnard & Greve (2016) in that we model the SLED integrated over all the cells in the simulation; each individual grid cell of the hydrodynamic simulation has its own smooth SLED. These integrated SLEDs, which are also smoothly varying, can be modeled by one component. Our approach also differs because Tunnard & Greve (2016) introduced slight errors on the lines produced by RADEX to better emulate real observations. We modeled the smoothly varying DESPOTIC-produced SLEDs without any added noise. This likely caused our integrated parameter uncertainties to be slightly smaller (bottom panel of Figure 6). Our uncertainties of approximately 0.2 dex should be considered the "best-case scenario" when 10 or more lines are available.

The precision drops significantly when only low-J lines are used (bottom panel of Figure 8). A vast range of physical conditions can produce the same low-J line emission. The distinguishing feature of the SLED is the point at which it turns over, usually in the mid-J region of our range. Without determining the approximate point of turnover and slope of the SLED after turnover (when plotted in luminosity units versus J-line), one cannot precisely determine the bulk physical

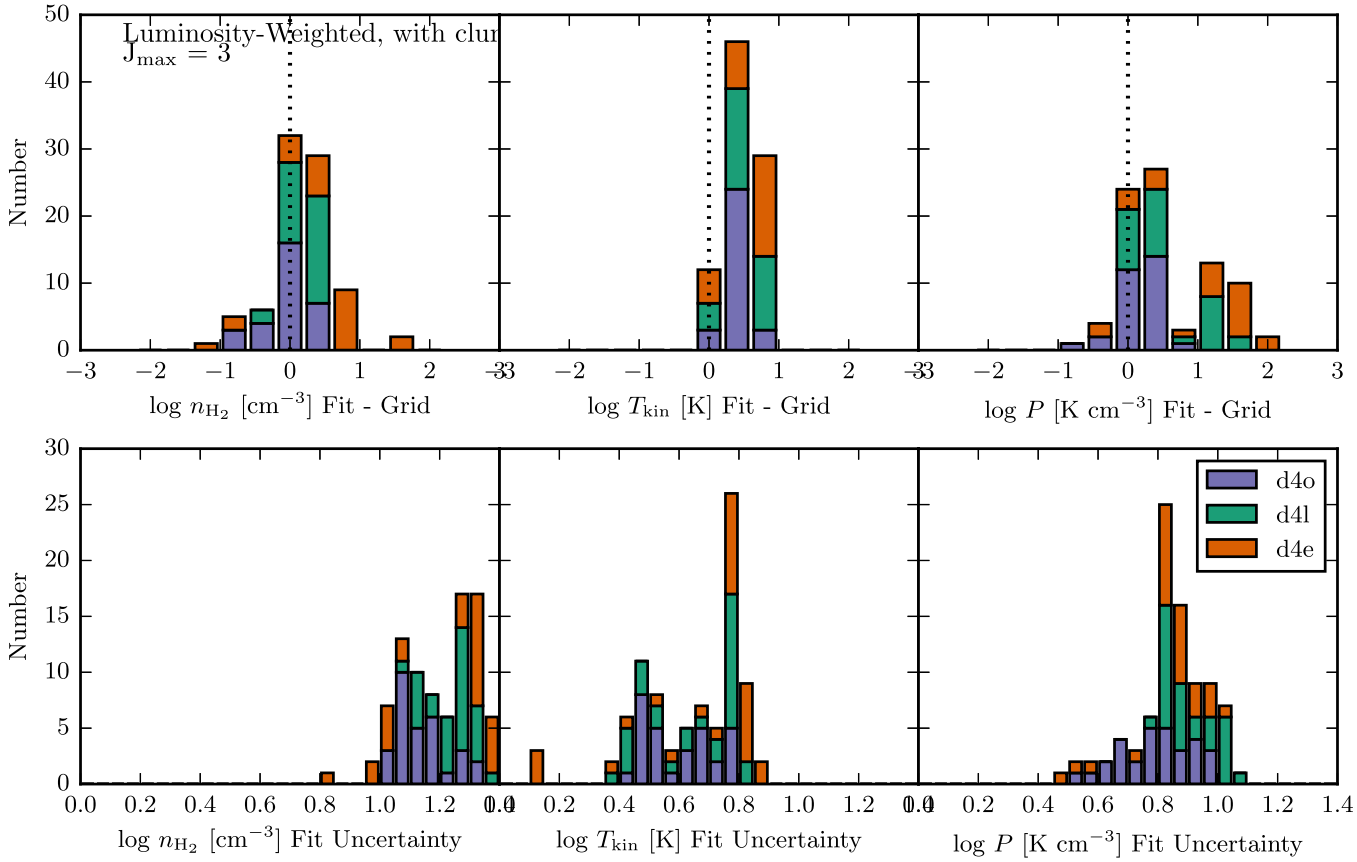

Figure 8. Top row: histogram of the difference between the luminosity-weighted and likelihood-fitted parameters, for only modeling up to $J = 3-2$. Bottom row: uncertainty (in dex) in the fitted parameters.

properties of the gas. Prior to ALMA and *Herschel*, this was the case for the majority of galaxies. Some high-J lines were available for bright galaxies under the best conditions (Papadopoulos et al. 2010, e.g., CO $J = 6-5$ from JCMT). The approximate uncertainties in the density, temperature, and their product (pressure) of 1.0–1.4, 0.4–0.8, and 0.8–1.0 dex, respectively, should be considered the "worst-case scenario" when only low-J lines are available.

Nearby galaxies observed with *Herschel* contain enough lines for modeling up to $J = 13-12$, but often require at least two unique components to fit the SLED, as was done in Kamenetzky et al. (2017). With two components comes a total of eight free parameters in the models; there is degeneracy between the cold and warm component parameters. The resulting uncertainties in the models, however, largely resemble what we find here (Figure 1 of Kamenetzky et al. 2017). The warm component, which is largely fit by the high-J lines, has a pressure uncertainty of about 0.3 dex. The cool component, which is largely fit by the low-J lines and is analogous to our low-J only models here, are uncertain to about 1.0 dex. The molecular mass, using a variety of methods, was found to be uncertain to a factor of about 0.4 dex on average (we do not focus on the molecular mass in this work). The uncertainty is larger, and result systematically offset (low), if the CO $J = 1-0$ line is absent, because the majority of the molecular mass is present in the ground state.

The recent progress made in the area of submillimeter observations of high-redshift galaxies offers a new, different challenge. A full CO SLED from $J = 1-0$ to $J = 10-9$ or $J = 13-12$ is rare and often difficult (Carilli & Walter 2013; Casey et al. 2014). For galaxies in the redshift range ~0.3–1.5 the $J = 1-0$ line is not accessible to sensitive facilities such as ALMA or the VLA, making the estimation of mass particularly uncertain. Which lines are available from ground-based observatories such as ALMA depend sensitively on the redshift. If at least a few lines are available that somewhat span the range from $J = 1-0$ through $J = 13-12$ (for example, a SLED with $J = 2-1$, $J = 5-4$, $J = 7-6$, which will likely encompass the SLED's turnover), the uncertainties in the physical conditions would likely be bracketed by our best-case scenarios (0.2 dex) and worst-case scenarios (1.0 dex). Of course, the best way to determine the parameters' uncertainties is to examine the relative likelihoods over a large parameter space using a nested-likelihood algorithm like we do here with MultiNest, or a Markov chain Monte Carlo (MCMC) method.

The second aspect of our question, that of accuracy, is harder to answer. What does it mean to accurately determine the bulk properties of a complex range of molecular gas clouds spanning an entire galaxy? As summarized in Leroy et al. (2017), the "density" of gas could refer to the collider density, critical density, effectively critical density (taking into account radiative line trapping), most effective density for emission, median density for emission, or median density by mass. Their modeled emission takes into account a realistic subresolution distribution of densities using log-normal and power-law distributions, but fix the temperatures and optical depths of all gas clouds to the same value. Even for a fixed temperature and optical depth, the emission of a molecular line varies with density. As Leroy et al. (2017) points out, regions with lower densities can still emit, but with lower efficiency. Lower-

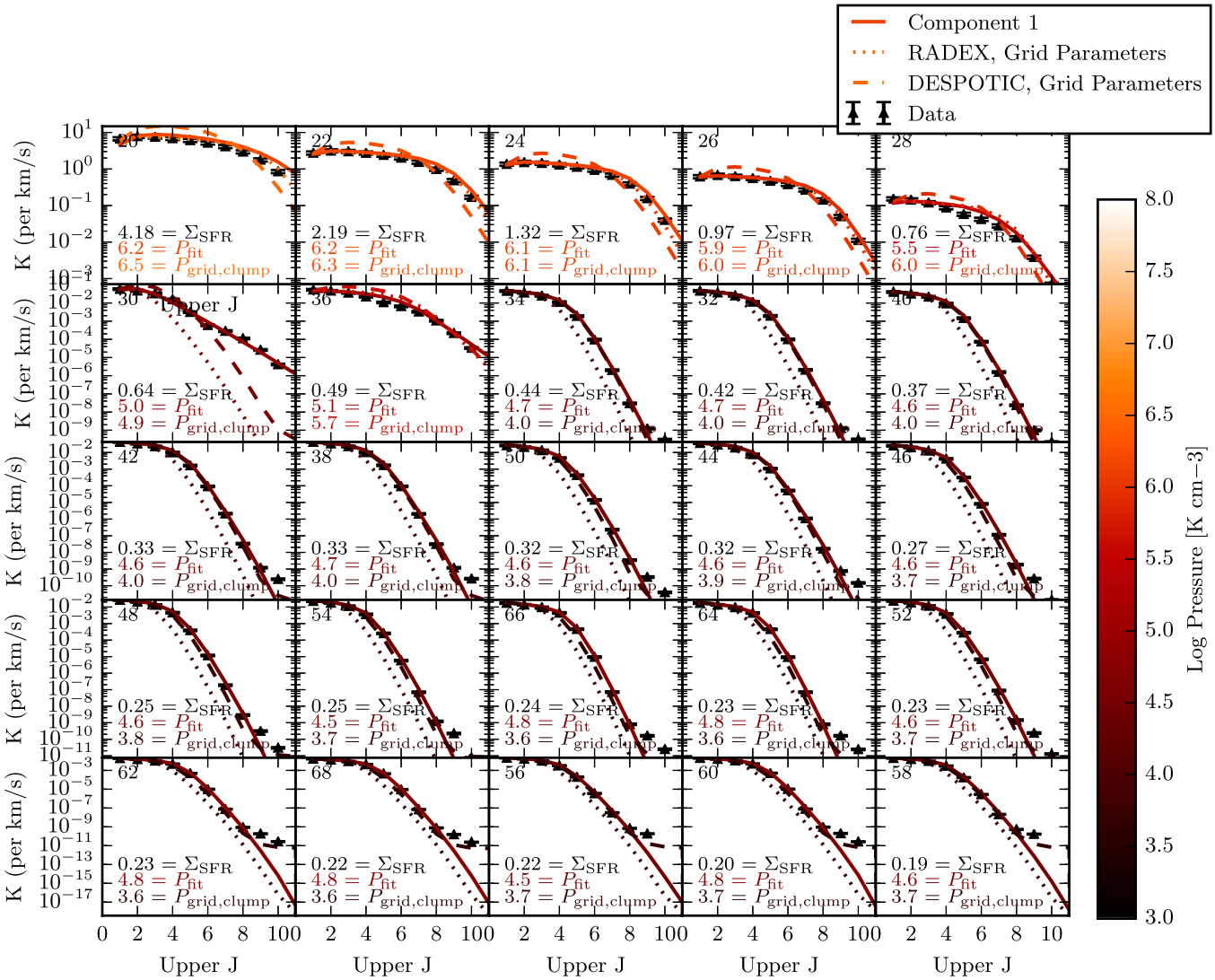

Figure 9. Spectral line energy distributions (SLEDs) for snapshots of d4e. Snapshots are in order from highest (upper left) to lowest (lower right) Σ_{SFR}. Each panel shows the galaxy-integrated SLED and the best-fit solution (solid line, color coded by pressure). We also show the RADEX and DESPOTIC (dotted and dashed) SLEDs using the luminosity-weighted temperature and density (effective clump density for RADEX) instead. We use the same column density and filling factor from the likelihood results. We fix them to the same $J = 1-0$ value as the best fit to better see the relative shapes.

density gas can contribute significantly to the total galaxy-integrated emission if it is present in a large enough amount. Our galaxy evolution simulations are more detailed in that they allow all properties (mass, temperature, density, and velocity dispersion) to vary on a cloud-by-cloud basis.

A clear conclusion of our work is that modeling of galaxy-integrated SLEDs does not accurately reproduce mass-weighted quantities, which are significantly lower in density, temperature, and velocity dispersion (Figure 2). Bulk properties derived from SLED fitting more accurately describe luminosity-weighted quantities. We find systematic offsets by property. For the gas density, our fitted parameters are systematically low (but not always, Figure 5). For the kinetic temperature, our fits are slightly systematically high. Both of these parameters are degenerate with one another, but their product (pressure) is often better determined. Our resultant pressures are much closer to the mass-weighted pressures from the simulation and follow the same general trend of increasing with Σ_{SFR} (Figure 4, bottom right). When using only the low-J lines, our median properties are systematically closer to the luminosity-weighted properties of the simulations, but as discussed previously, the uncertainties were much higher.

This demonstrates that the beam-integrated emission from galaxies is dominated by the brightest, most extremely excited molecular gas. Such highly excited gas represents a small fraction of the total mass, consistent with the findings of Kamenetzky et al. (2014). For only the smallest Σ_{SFR} snapshots studied here was there a difference between properties weighted by $J = 8-7$ versus total CO luminosity. For these scenarios, the high-J emission alone greatly weights the total integrated SLEDs.

5. Conclusions

Any CO SLED integrated over a large area is the sum of a gradient in physical conditions (temperature and density). Given a large number of free parameters for each component of gas (temperature, density, column density, and area filling factor) and often a small number of molecular line luminosities available for fitting, observers must necessarily model the smallest number of components to make statistically robust

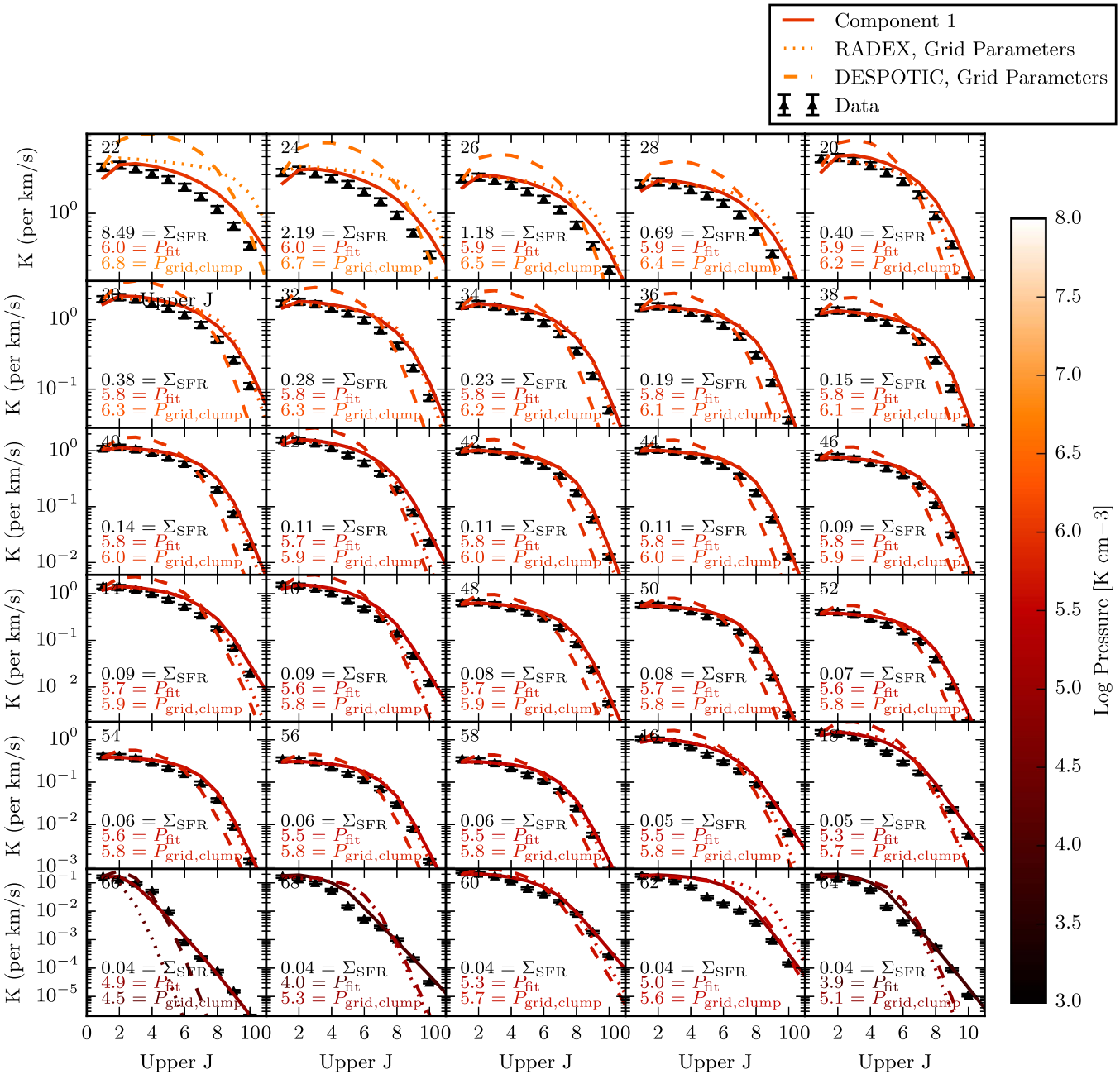

Figure 10. Spectral line energy distributions (SLEDs) for snapshots of d4o. See the caption of Figure 9.

conclusions. These components (usually one, two, or occasionally three) are an oversimplification of a complex galactic system. We sought to take a computational model of such a complex galactic system and "compress" its information into one total integrated SLED, as an observer would see, and then model the gas as observers do. Our main conclusions are as follows:

1. When fitting CO SLEDs as a discrete number of components, the resultant parameters should be considered analogous to luminosity-weighted parameters, not mass-weighted. The highest luminosity regions of galaxy SLEDs represent the most excited conditions, but a small fraction of the mass.
2. For large Σ_{SFR} snapshots, the luminosity-weighted parameters (temperature, density, and pressure) were the same whether we weighted by CO $J=8-7$ or the total CO luminosity. For small Σ_{SFR}, however, weighting by CO $J=8-7$ resulted in slightly higher temperatures, densities, and pressures, indicating that high-J emission has a greater influence on the SLED when Σ_{SFR} is low
3. When only using low-J lines ($J=1-0$, $J=2-1$, and $J=3-2$), the uncertainties in the derived physical quantities are approximately one order of magnitude. The true luminosity-related quantities generally fall within the range of uncertainty.
4. On the other hand, when fitting the first 10 rotational lines, the uncertainty is usually about 0.2 dex, through the true luminosity-weighted densities, temperatures and pressures generally fall outside this range of uncertainty. This indicates a systematic difference between our recovered properties and the true luminosity-weighted

properties, though they are close. An uncertainty of 0.2 dex is likely to be a lower limit on the uncertainty, as SLEDs are rarely more well sampled than with data covering the first 10 rotational lines.

5. We therefore suggest that the typical systematic uncertainty on the physical properties when SLED modeling lies between 0.2 and 1 dex., depending on the number of lines modeled, the sampling of the SLED in energy space, and the uncertainties of the integrated line fluxes.

J.K. was supported by the National Science Foundation under Grant Number AST-1402193. G.C.P. acknowledges support from a FONDECYT Postdoctoral Fellowship (No. 3150361) and from the University of Florida. G.C.P. thanks the Sexten Center for Astrophysics (http://www.sexten-cfa.eu) where part of this work was performed. Partial support for D.N. was provided by NASA *HST* AR-13906.001, *HST* AR-15043.0001, NSF AST-1724864, and NSF AST-1715206. The Cosmic Dawn Center is funded by the Danish National Research Foundation.

Software: RADEX (van der Tak et al. 2007), PyRadex (https://github.com/keflavich/pyradex), MultiNest (Feroz et al. 2009), PyMultiNest (Buchner et al. 2014), PyRadexNest (Kamenetzky 2018), DESPOTIC (Krumholz 2013).

ORCID iDs

J. Kamenetzky https://orcid.org/0000-0001-7877-7942
G. C. Privon https://orcid.org/0000-0003-3474-1125
D. Narayanan https://orcid.org/0000-0002-7064-4309

References

Bayet, E., Bureau, M., Davis, T. A., et al. 2013, MNRAS, 432, 1742
Bolatto, A. D., Leroy, A. K., Rosolowsky, E., Walter, F., & Blitz, L. 2008, ApJ, 686, 948
Bolatto, A. D., Wolfire, M., & Leroy, A. K. 2013, ARA&A, 51, 207
Buchner, J., Georgakakis, A., Nandra, K., et al. 2014, A&A, 564, A125
Carilli, C., & Walter, F. 2013, ARA&A, 51, 105
Casey, C. M., Narayanan, D., & Cooray, A. 2014, PhR, 541, 45
Daddi, E., Dannerbauer, H., Liu, D., et al. 2015, A&A, 577, A46
Feroz, F., Hobson, M. P., & Bridges, M. 2009, MNRAS, 398, 1601
Greve, T. R., Leonidaki, I., Xilouris, E. M., et al. 2014, ApJ, 794, 142
Hernquist, L. 1990, ApJ, 356, 359
Kamenetzky, J. 2018, jrka/pyradexnest PyRadexNest v1.0, Zenodo, doi:10.5281/zenodo.1135261
Kamenetzky, J., Rangwala, N., & Glenn, J. 2017, MNRAS, 471, 2917
Kamenetzky, J., Rangwala, N., Glenn, J., Maloney, P. R., & Conley, A. 2014, ApJ, 795, 174
Kamenetzky, J., Rangwala, N., Glenn, J., Maloney, P. R., & Conley, A. 2016, ApJ, 829, 93
Kennicutt, R. C., Jr. 1998, ARA&A, 36, 189
Kennicutt, R. C., & Evans, N. J. 2012, ARA&A, 50, 531
Krumholz, M. R. 2013, MNRAS, 437, 1662
Krumholz, M. R., McKee, C. F., & Tumlinson, J. 2008, ApJ, 689, 865
Krumholz, M. R., McKee, C. F., & Tumlinson, J. 2009a, ApJ, 693, 216
Krumholz, M. R., McKee, C. F., & Tumlinson, J. 2009b, ApJ, 699, 850
Lemaster, M. N., & Stone, J. M. 2008, ApJL, 682, L97
Leroy, A. K., Usero, A., Schruba, A., et al. 2017, ApJ, 835, 217
Lu, N., Zhao, Y., Díaz-Santos, T., et al. 2017, ApJS, 230, 1
McKee, C. F., & Ostriker, J. P. 1977, ApJ, 218, 148
Meijerink, R., Kristensen, L. E., Weiß, A., et al. 2013, ApJL, 762, L16
Mo, H. J., Mao, S., & White, S. D. M. 1998, MNRAS, 295, 319
Narayanan, D., Krumholz, M., Ostriker, E. C., & Hernquist, L. 2011, MNRAS, 418, 664
Narayanan, D., & Krumholz, M. R. 2014, MNRAS, 442, 1411
Narayanan, D., & Krumholz, M. R. 2017, MNRAS, 467, 50
Narayanan, D., Krumholz, M. R., Ostriker, E. C., & Hernquist, L. 2012, MNRAS, 421, 3127
Ostriker, E. C., Stone, J. M., & Gammie, C. F. 2001, ApJ, 546, 980
Padoan, P., & Nordlund, Å. 2002, ApJ, 576, 870
Papadopoulos, P., Van Der Werf, P., Isaak, K. G., & Xilouris, E. 2010, ApJ, 715, 775
Papadopoulos, P. P., Zhang, Z.-Y., Xilouris, E. M., et al. 2014, ApJ, 788, 153
Rosenberg, M. J. F., van der Werf, P. P., Aalto, S., et al. 2015, ApJ, 801, 72
Schirm, M. R. P., Wilson, C. D., Parkin, T. J., et al. 2014, ApJ, 781, 101
Schmidt, M. 1959, ApJ, 129, 243
Sliwa, K., Wilson, C. D., Petitpas, G. R., et al. 2012, ApJ, 753, 46
Solomon, P. M., Rivolo, A. R., Barrett, J., & Yahil, A. 1987, ApJ, 319, 730
Spilker, J. S., Marrone, D. P., Aguirre, J. E., et al. 2014, ApJ, 785, 149
Springel, V., Di Matteo, T., & Hernquist, L. 2005, MNRAS, 361, 776
Springel, V., & Hernquist, L. 2002, MNRAS, 333, 649
Springel, V., & Hernquist, L. 2003, MNRAS, 339, 289
Strandet, M. L., Weiss, A., De Breuck, C., et al. 2017, ApJL, 842, L15
Tunnard, R., & Greve, T. R. 2016, ApJ, 819, 161
van der Tak, F. F. S., Black, J. H., Schöier, F. L., Jansen, D. J., & van Dishoeck, E. F. 2007, A&A, 468, 627
Weiß, A., Downes, D., Neri, R., et al. 2007, A&A, 467, 955
Wolfire, M. G., Hollenbach, D., & McKee, C. F. 2010, ApJ, 716, 1191
Xu, C. K., Cao, C., Lu, N., et al. 2015, ApJ, 799, 11